Numerical Analysis of the Interaction between Thermo-Fluid Dynamics and Auto-Ignition Reaction in Spark Ignition Engines*

Katsuya SAIJYO**, Kazuie NISHIWAKI***
and Yoshinobu YOSHIHARA***

The CFD simulations were performed integrating the low-temperature oxidation reaction. Analyses were made with respect to the first auto-ignition location in the case of a premixed-charge compression auto-ignition in a laminar flow field and in the case of the auto-ignition in an end gas during an S.I. Engine combustion process. In the latter simulation, the spatially-filtered transport equations were solved to express fluctuating temperatures in a turbulent flow in consideration of strong non-linearity to temperature in the reaction equations. It is suggested that the first auto-ignition location does not always occur at higher-temperature locations and that the difference in the locations of the first auto-ignition depends on the time period during which the local end gas temperature passes through the region of shorter ignition delay, including the NTC region.

Key Words: Ignition, Premixed Combustion, Internal Combustion Engine, CFD, Knock

1. Introduction

Observations of knocking in S. I. Engines via high-speed photography[1][2] revealed knocking to initiate coincident with the appearance of several bright spots in close proximity to the walls. This tendency is not clearly understood, because the gas temperatures in the wall boundary layer are lower than those in the core region (distant from the wall). Some experiments[3][4] showed the appearance of several bright spots upon auto-ignition in the end gas zone at a distance from the cylinder liner. Another experiment[5] using a multi-optical fiber technique indicated that several luminous sites were detected both near the flame front and near the liner wall.

Several CFD studies[6] ~ [8] integrated the auto-ignition reaction for knocking simulation. However, the results of these studies were unsatisfactory in reproducing such behaviors of auto-ignition as observed in these experiments, showing one comparatively large hot region in the end gas outside the thermal boundary layer. All of these simulations relied on the Reynolds-averaged transport equations using the k-ε turbulence model, and solved the phase-averaged variables that eliminate fluctuating components. As the reaction kinetics equations have strong non-linearity with respect to temperature, the reaction rates obtained from the phase-averaged temperatures must be different from those obtained from fluctuating temperatures.

The spatially-filtered transport equations simulate temporal and spatial fluctuations in dependent variables with the spatial resolution of a numerical cell size in a turbulent field. Therefore, the spatially-filtered transport equations are a reasonable choice for providing temperatures for the reaction

* Received 20th May, 2002 (No. 02-4086)
** Graduate School, Ritsumeikan University, 1-1-1 Nojihigashi, Kusatsu, Shiga 525-8577, Japan. E-mail: mpe40036@se.ritsumei.ac.jp
*** Department of Mechanical Engineering, Ritsumeikan University. E-mail: nswk@se.ritsumei.ac.jp

terms. In addition, the spatially-filtered transport equations have the potential to simulate the random nature of the appearance of the auto-ignition spots.

The purpose of the present study is to analyze reason why the first local auto-ignition is observed near the wall in some cases and at a distance from the wall in other cases. First, an analysis of a compression ignition in a rapid compression machine in a laminar state is performed in order to gain a basic understanding of the interaction between fluid flow and the auto-ignition reaction. Second, the auto-ignition in the end gas in an S. I. engine in a three-dimensional turbulent field is investigated by solving the spatially-filtered transport equations.

2. A Reduced Kinetic Model for Low Temperature Oxidation

Cowart et al.[9] developed a reduced kinetic mechanism for the low-temperature oxidation of hydrocarbons, which consists of nineteen reactions. The model features that the activation energy of the forward rate of the isomerization reaction is the only empirical constant for different fuels. The number of reaction equations is practically acceptable from the viewpoint of computational time when integrated in CFD code. The model, however, showed a rather slow increase in temperature at the transition from the low-temperature oxidation to the hot-flame reaction. The original model was modified at Ritsumeikan University[10)~(12)] to produce a rapid increase. The details of this modification are shown in Refs. (10) and (11). Basically, the modification introduced a reverse path for the radical recombination reaction. In addition to this modification, the rate constants of the isomerization and the third-body reactions were adjusted to fit the experimental ignition delays for i-octane presented by Halstead et al.[13]

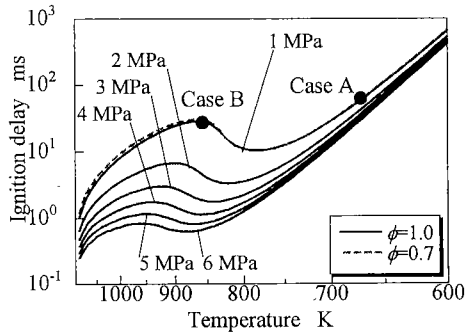

Figure 1 The ignition delay as a function of temperature calculated by the modified MIT model[10)~(12)] for a primary reference fuel of octane number 90, covering the equivalence ratios ϕ and the pressure range in the present study

The ignition delay under constant pressure was calculated using the modified model for the constant-volume vessel, using the thermodynamic zero-dimensional calculation. The ignition delay was defined as the time period from the calculation start to the time at which the temperature reaches 1100 K. A primary reference fuel of octane number 90(mixture of 90 vol% of i-octane and 10 vol% of n-heptane) was used in the present study. The activation energy of the forward rate of the isomerization reaction for this fuel was taken from the experimental result of Foin et al.[12] Figure 1 shows the ignition delay with respect to temperature, for the equivalence ratio and pressure range examined in the present study.

3. Compression Ignition in a Laminar State in a Rapid Compression Machine

In order to gain a basic understanding of the interaction between thermo-fluid dynamics and the auto-ignition reaction, calculations were performed for a compression ignition in a rapid compression machine having a disc shaped combustion chamber. The cylinder bore and stroke were 65 mm and 141 mm, respectively. The flow field was assumed to be laminar throughout the process. The general conservation equations of mass, momentum, enthalpy and species concentrations were solved in an axisymmetric field. The numerical grid has 60 nodes in the radial direction. In the axial direction, the grids contract with piston motion, and the number of nodes was reduced by half at two selected crank angles, resulting in the number of nodes being reduced from 160 to 40 during compression.

The calculation was performed for a homogeneous mixture of a primary reference fuel of octane number 90 and air having an equivalence ratio of 0.7. The compression ratio was set to be 7.13. The wall temperature was assumed to be 368 K. The piston motion was that of the crank-piston mechanism of an engine. The compression speed was set to be 750 rpm, and the piston stopped at TDC. The calculations were started at BDC at the pressure p_i=0.075 MPa using a stationary mixture charge. The initial temperature T_i was assumed to be uniform throughout the volume, and two different conditions T_i =343 K (Case A) and 463 K (Case B) were investigated. The calculation was terminated when the temperature reached 1100 K at any location. At the end of compression, the calculated pressures were approximately 1 MPa in both cases, and the cylinder volume-averaged temperatures were 677 K for Case A and 855 K for Case B. These conditions were plotted on the ignition delay curve at a

pressure of 1 MPa in Figure 1, which shows that Case A is in a lower temperature region outside the negative temperature coefficient (NTC) region and Case B is near the higher temperature end of the NTC region.

Figure 2 shows velocity vectors and temperature fields at several selected crank angles before auto-ignition in Case A. The velocity vectors are depicted by radial velocity component and the axial velocity component relative to the moving grid. It is seen that the roll-up vortex is induced in the piston-liner corner during compression. At the end of compression, the roll-up vortex penetrates the central region and develops into a clockwise rotation. The size of the roll-up vortex is known to be much larger in a laminar state than in a turbulent state[14], and this is reflected by the calculation results. In this process, the vortex loses heat due to wall heat transfer to generate a comparatively large temperature difference between the central and outer regions. A difference of approximately 100 K or more can be seen.

Figure 3 shows the fields of temperature and local heat release rate in Case A at the first local auto-ignition or 38.4 ms after the end of compression. In this case, all the local temperatures are lower than the NTC region at the end of compression, as shown in Figure 2. As expected, the higher-temperature region or the outer region from the cylinder axis comes to the first auto-ignition, as seen in the left-hand side of Figure 3. Correspondingly, the local heat release rates,

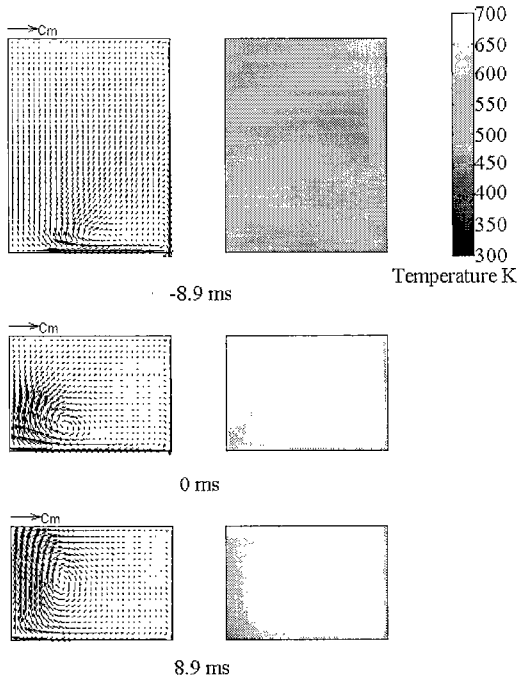

Figure 2 The velocity vector (left) and temperature (right) fields at several selected crank angles for T_i=343 K; 0 ms : end of compression

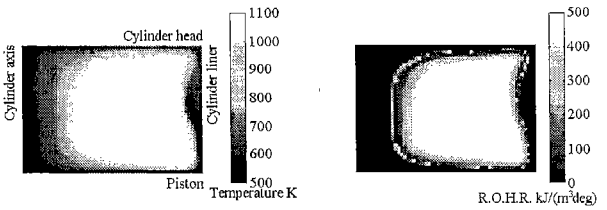

Figure 3 The fields of temperature (left) and local heat release rate (right) for initial temperature T_i=343 K, at the first local auto-ignition, 38.4 ms.

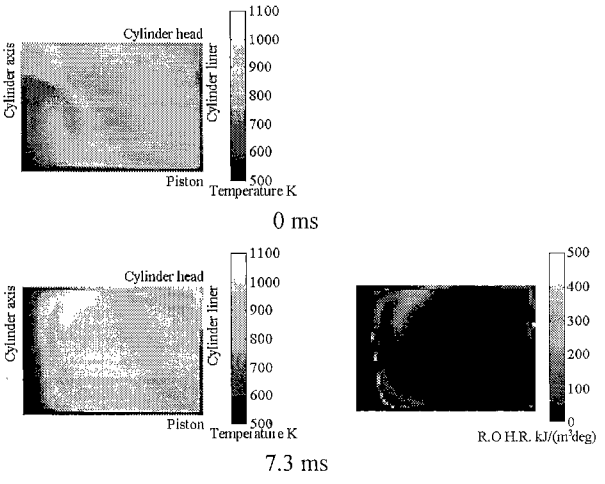

Figure 4 The temperature field at the end of compression (0 ms), and the fields of temperature and local heat release rate at 7.3 ms or the first local auto-ignition for the initial temperature T_i=463 K

shown in the right-hand side of Figure 3, are higher in the outer region. It is seen that the locations of higher local heat release rate form a chain around the outer region in the cool flame reaction phase before the hot flame reaction.

The upper part of Figure 4 shows the temperature field at the end of compression in Case B. The temperatures range roughly from 500 K to 890 K, which include the NTC region. Shown in the lower part of the figure are the temperature and the local heat release rate fields at the first local auto-ignition or 7.3 ms after the end of compression. It is seen that the auto-ignition begins at the border between the higher- and lower-temperature regions, including the near wall regions.

As described above, the first local auto-ignition takes place at various locations, depending on whether the local temperatures are outside the NTC region or cover the NTC region. In both cases, the thick ring-like shape of the local heat release rates will be observed when looking down from the cylinder head, which is

similar to the blue flame observation presented by Furutani and Ohta[15].

4. Three-dimensional Analysis of Auto-ignition in an S. I. Engine Combustion Process

The auto-ignition sites are generated in the process of spatial and temporal fluctuations in velocity, temperature and fuel concentration. Therefore, the fluctuating nature of turbulence should be taken into consideration in the analysis of a three-dimensional field of a spark-ignition combustion process.

The transport equations to be solved are expressed in a spatially Favre-filtered form in a sub-grid scale for momentum, enthalpy h, species concentrations Y_i and progress variable c. These are given as follows:

$$\frac{\partial}{\partial t}(\bar{\rho}\,\tilde{u}_i)+\frac{\partial}{\partial x_k}(\bar{\rho}\,\tilde{u}_k\,\tilde{u}_i)-\frac{\partial}{\partial x_k}\left(\mu\bar{S}_{ik}+2\bar{\rho}\nu_S\tilde{S}_{ik}\right)=-\frac{\partial p}{\partial x_i} \quad \cdots\cdots(1)$$

$$\frac{\partial}{\partial t}(\bar{\rho}\,\tilde{h})+\frac{\partial}{\partial x_k}(\bar{\rho}\,\tilde{u}_k\,\tilde{h})-\frac{\partial}{\partial x_k}\left(\lambda\frac{\partial\bar{T}}{\partial x_k}+\bar{\rho}\nu_S\frac{\partial\tilde{h}}{\partial x_k}\right)=\frac{d\bar{p}}{dt}+\tilde{X}_u\dot{Q}_R+Y_{fu,u}H_L\omega \quad \cdots\cdots(2)$$

$$\frac{\partial}{\partial t}(\bar{\rho}\,\tilde{Y}_i)+\frac{\partial}{\partial x_k}(\bar{\rho}\,\tilde{u}_k\,\tilde{Y}_i)-\frac{\partial}{\partial x_k}\left(\mu\frac{\partial\tilde{Y}_i}{\partial x_k}+\bar{\rho}\nu_S\frac{\partial\tilde{Y}_i}{\partial x_k}\right)=R_i-\frac{\tilde{Y}_i}{\tilde{Y}_u}\omega \quad \cdots\cdots(3)$$

$$\frac{\partial}{\partial t}(\bar{\rho}\,\tilde{c})+\frac{\partial}{\partial x_k}(\bar{\rho}\,\tilde{u}_k\tilde{c})-\frac{\partial}{\partial x_k}\left(\mu\frac{\partial\tilde{c}}{\partial x_k}+\bar{\rho}\nu_S\frac{\partial\tilde{c}}{\partial x_k}\right)=\omega \quad \cdots\cdots(4)$$

$$S_{ij}=\frac{1}{2}\left(\frac{\partial u_j}{\partial x_i}+\frac{\partial u_i}{\partial x_j}\right) \quad \cdots\cdots(5)$$

where ρ is the density, u_i is the velocity component, p is the pressure, μ is the molecular viscosity, λ is the thermal conductivity, X_u is the volume fraction of unburned mixture, $\dot{Q}_R$ is the heat release rate from low temperature oxidation, $Y_{fu,u}$ is the fuel mass fraction in unburned mixture, H_L is the lower heating value, ω is the burning rate, Y_u is the mass fraction of unburned mixture and R_i is the production rate of species concentration due to the chemical reaction in unburned mixture. In the above equations, the over bar "$\bar{\ }$" indicates a spatially-filtered quantity, and the tilde over bar "~" denotes a spatially-Favre-filtered quantity. The symbol ν_S is sub-gird kinematic viscosity expressed by the Smagorinsky model in the form:

$$\nu_S=(C_S\Delta)^2\left(2\tilde{S}_{ij}\tilde{S}_{ij}\right)^{1/2} \quad \cdots\cdots(6)$$

where, C_S is a model constant set to 0.2; Δ is the filter length given by the cubic root of a cell volume.

A model for the burning rate should also have a spatially-averaged nature of the turbulent flame propagation in a cell size. The averaged behavior in space is assumed to be equal to that in time in a turbulent flow field. In the present study, Weller's model[16], which was presented in Reynolds-averaged or time-averaged form, was adopted. The burning rate ω in a spatially-averaged form within a cell may be expressed in the following form:

$$\omega=A\bar{\rho}_u S_T|\nabla\tilde{c}| \quad \cdots\cdots(7)$$

where A is an empirical constant, ρ_u is the unburned mixture density, and S_T is the turbulent burning velocity averaged over a cell volume. The turbulent flame structure is derived from the concept of fractal geometry. The ratio of turbulent burning velocity S_T to laminar burning velocity S_L is expressed in the following form using fractal dimension D:

$$\frac{S_T}{S_L}=\left(\frac{L_i}{\Delta}\right)^{2-D} \quad \cdots\cdots(8)$$

where, L_i is the inner cutoff scale. Note that Eq. (8) is written by replacing the outer cutoff scale with Δ in the form S_T/S_L in the fractal model for the Reynolds-averaged burning rate. Based on the experimental result of Gülder et al.[17], the fractal dimension D was assumed to be 2.2. The inner cutoff scale L_i was assumed to be the Kolmogorov scale η, which is expressed by:

$$L_i=\eta=\left(\nu^3/\varepsilon_S\right)^{1/4} \quad \cdots\cdots(9)$$

The dissipation rate ε_S can be written from the dimensional analysis in the following form:

$$\varepsilon_S=B\nu_S^3/\Delta^4 \quad \cdots\cdots(10)$$

where B is a model constant.

Equations (8), (9) and (10) are introduced into Eq.(7) to yield:

$$\omega = A'\bar{\rho}_u S_L \left(\frac{\nu}{\nu_S}\right)^{-0.15} |\nabla\tilde{c}| \quad ; \quad A' = AB^{0.05} \qquad \cdots\cdots(11)$$

where A' is an empirical constant and was adjusted to 1.86 so that a computed pressure would fit the experimental results.

The equation for unburned mixture enthalpy[18] is added to the above equations to obtain temperature of unburned mixture in a cell containing a burned gas.

When Y_u approaches zero, the right hand side of Eq. (3) becomes unstable. In order to avoid this, the right hand side of Eq. (3) was set zero in the cells in which Y_u is 0.1 or less, as an amount of the species generated in the auto-ignition reaction is negligible under these conditions.

The wall shear force and the wall heat flux were given by the law of the wall. The wall boundary condition for species and progress variable were given by a zero gradient normal to the wall.

The engine used for the present calculation was a modified CFR engine having a spark plug located at the center of the cylinder head surface. The engine speed was 900 rpm and spark timing was 30 deg. BTDC. The fuel was a primary reference fuel of octane number 90, and the air/fuel ratio was set to be stoichiometric.

The following considerations were taken into account when setting the initial turbulent flow field. The experiments involving almost practical engines showed that the auto-ignition spots appeared in close proximity to the walls[1][5] and sometimes in the core region[3][4][5]. In the experiment involving a spark-ignition combustion in a rapid compression machine[2], the auto-ignition initiated very near the wall. Thus the location of the auto-ignition does not depend on the existence (in the practical engines) or non-existence (in the RCM) of average flows at the initial. Based on this finding, a simple turbulent flow field was analyzed in order to gain a basic understanding.

In order to save computational time and still obtain reasonable results, calculations were begun at 60 deg. BTDC with the initial condition provided by the axisymmetric computations of the Reynolds averaged transport equations using the k-ε two-equation turbulence model. The calculations of the Reynolds averaged equations were started at intake valve closing (135 deg. BTDC) using the initial turbulence kinetic energy of $k = 0.74C_m^2$ (C_m: mean piston speed)[19], resulting in a volume average of $k_{60\,BTDC} = 0.29C_m^2$ at 60 deg. BTDC. Fluctuations in each velocity component, u', were generated by uniform random numbers so as to satisfy the following relation:

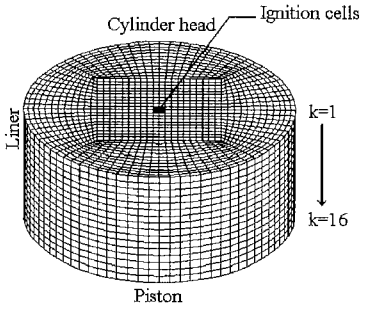

Figure 5 Computational grid systems

$$|u'| \le \sqrt{3}\left(\frac{2}{3}k_{60\,BTDC}\right)^{1/2} \qquad \cdots\cdots(12)$$

The fluctuations u' were added at 60 deg. BTDC to the assumed turbulence averaged velocity, which has an axial component ranging from zero at the surface of the cylinder head to the piston speed at the piston face; the other two components being zero. This flow field neglects the vortex induced in a piston-liner corner before 60 deg. BTDC, though the vortex plays an important role in the preceding analysis of the laminar case. However, the size of the vortex is much smaller in a turbulent state than in a laminar state[14]. In addition, strong flows induced by flame propagation are dominant during the combustion process. Therefore, the vortex effect can be treated as a minor factor in the present analysis.

Temperature, pressure and residual gas mass fraction were assumed to be uniform at 60 deg. BTDC and were given by the results of a zero-dimensional cycle simulation including a gas-exchange process having an intake port pressure of 0.099 MPa and an intake port temperature of 325 K. Here, the temperature, pressure and residual gas mass fraction were 593 K, 0.33 MPa and 0.1, respectively. The fuel/air ratio was stoichiometric and was assumed to be uniform. The wall temperature, determined experimentally as 433 K, was assumed to be uniform over all walls.

Figure 5 illustrates the numerical grids for the combustion chamber. The number of cells is 44x44x16, which gives an average grid size of 2 mm. The axial coordinate contracts and expands as the piston moves. Spark ignition was modeled by instantaneous combustion of 25% of the fuel in the four ignition cells, as shown in the figure. The calculation was terminated when the unburned mixture temperature reached 1100 K at any location.

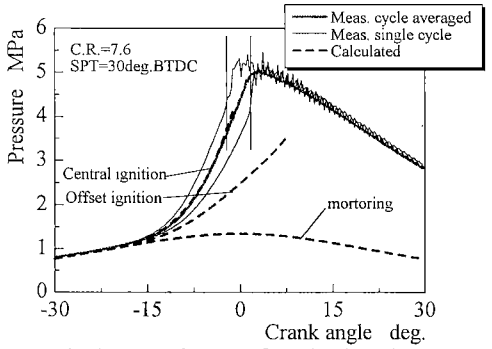

Figure 6 Comparison of calculated pressure with experimental results

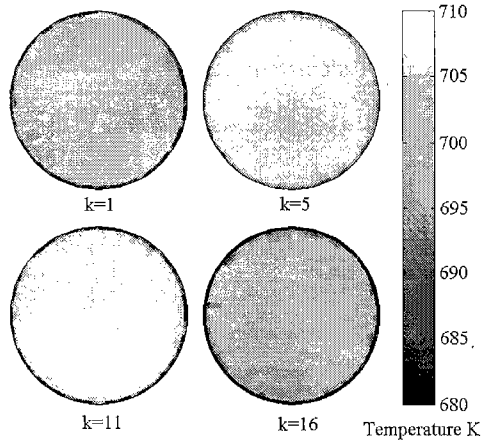

Figure 7 Calculated temperature fields at 35 deg. BTDC (before ignition)

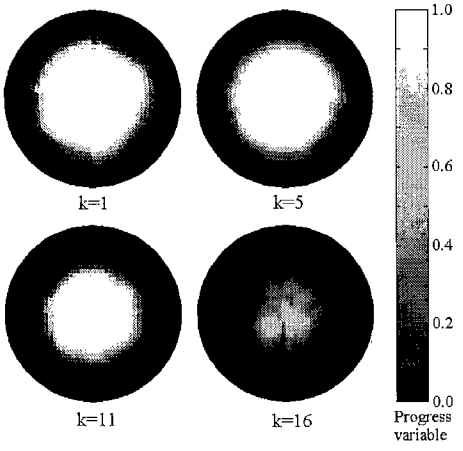

Figure 8 Calculated progress variable fields at 10 deg. BTDC

Figure 6 compares the calculated pressure and the experimentally obtained pressure. The thick solid line indicates a cycle-averaged pressure curve, and the thin lines are two typical curves of individual cycles. The dashed line is the calculated pressure. It is seen that the predicted time of knock initiation falls into the range of the fluctuating experimental results.

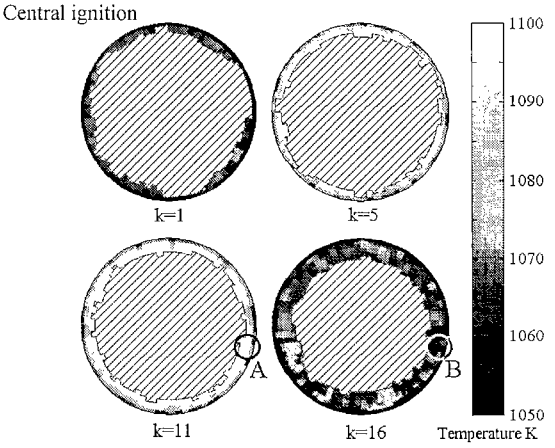

Figure 9 Calculated temperature fields of unburned mixture at 1.1 deg. BTDC (first local auto-ignition); Central ignition

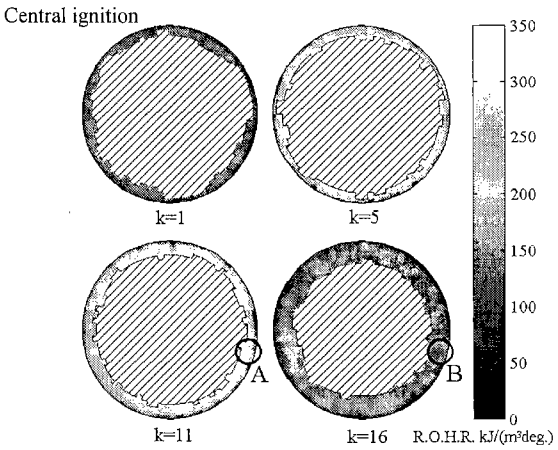

Figure 10 Calculated local heat release rates from low temperature oxidation at 1.1 deg. BTDC (first local auto-ignition); Central ignition

The temperature fields calculated at 35 deg. BTDC (before ignition) are shown in Figure 7. The planes perpendicular to the cylinder axis are referred to by k-number, as illustrated in Figure 5. It is noted that temperature fluctuations appear in the near-wall regions despite the uniform temperature field given as the initial condition. This is due to temporal and spatial variations in wall heat transfer generated by random flow motion.

Calculated progress variable fields at 10 deg. BTDC are presented in Figure 8. Wrinkles of cell size seen in the flame front is due to the randomly fluctuating flow.

Figure 9 shows the calculated temperature fields of unburned mixture at 1.1 deg. BTDC or first local auto-ignition. The hatched area in each plane indicates burned gas, the temperature of which is not shown. Several sites can be seen to reach or almost reach

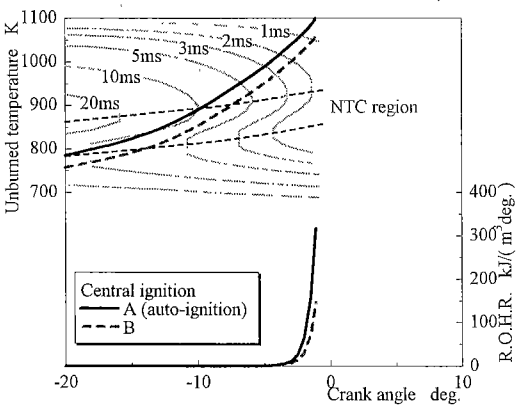

Figure 11 Time histories of temperatures and local heat release rate at the first local auto-ignition cell (location A) and near wall cell (location B); Central ignition

auto-ignition sporadically at locations distant from the walls, but not in the near-wall regions. Comparing the temperatures and local heat release rates shown in Figure 10, the locations of stronger local heat release rate almost coincides with the locations of higher temperature.

Figure 11 shows the time histories of temperatures and local heat release rates at the first local auto-ignition cell (location A in Figures 9 and 10) and at a near-wall cell (location B in Figures 9 and 10), with contours of ignition delay as a function of temperature and pressure. It is seen that the temperatures at both the locations pass through the NTC region, in which location B is faster with respect to reaction. However, a difference in the ignition delay and a time period in the NTC region are not sufficient for location B to overtake location A.

In order to observe differences in the appearance of the auto-ignition sites, another calculation was performed for the offset spark ignition located 36 mm from the cylinder center, while the other conditions were the same. Although no experimental result was available in this case, an analysis based on the preceding discussion will be useful as a basic concept. The calculated pressure is shown in Figure 6, exhibiting slower combustion than in the case of the central spark. The first local auto-ignition is seen at 7.2 deg. ATDC. The temperature fields of the unburned mixture at this time are shown in Figure 12. It can be seen that the first local auto-ignition appears in the piston-liner corner (plane k=16), at location D. The locations at which the temperatures are between 1090 K and 1100 K are marked by a hollow triangle to indicate the locations that are approaching auto-ignition. As shown in Figure 13, the local heat release rates at these locations exhibit higher values. Large parts of the unburned mixture that are distant

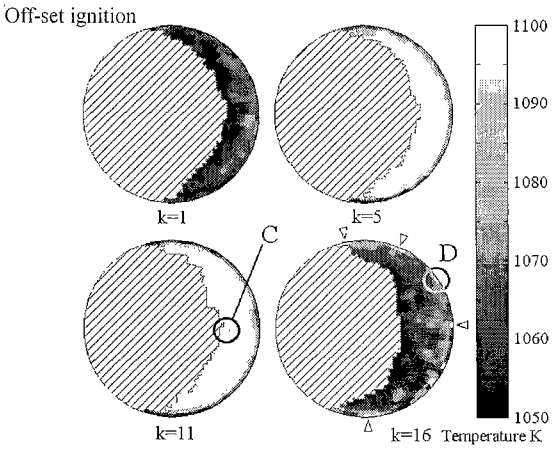

Figure 12 Calculated temperature fields of unburned mixture at 7.2 deg. BTDC (first local auto-ignition); Off-set ignition

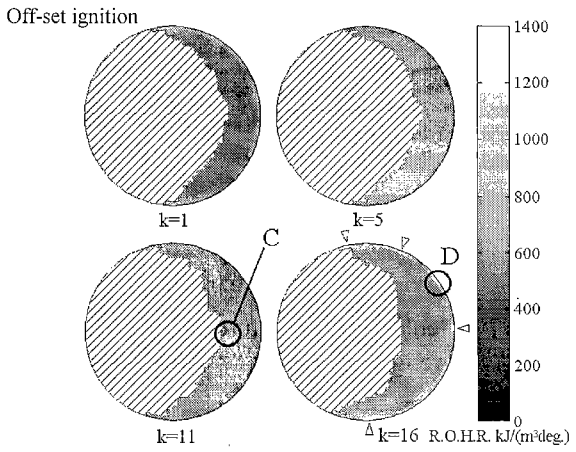

Figure 13 Calculated local heat release rates from low temperature oxidation at 7.2 deg. BTDC (first local auto-ignition); Off-set ignition

from the wall in the planes k=5 and k=11 are in the temperature range between 1090 K and 1100 K, as shown in Figure 12. Immediate auto-ignition also occurs at these locations. However, the local heat release rates are much lower than those of the auto-ignition sites in the piston-liner corner.

Figure 14 shows the time histories of temperatures and local heat release rates at a core region cell (location C in Figures 12 and 13) and the first local auto-ignition cell (location D in Figures 12 and 13). As seen in the figure, the temperature at location D passes through the NTC region and exceeds that at location C to reach auto-ignition. This behavior can be explained as follows. Location D passes through the condition, including the NTC region, in which the ignition delay is shorter than at location C. The time under this condition is long enough for location D to overtake location C.

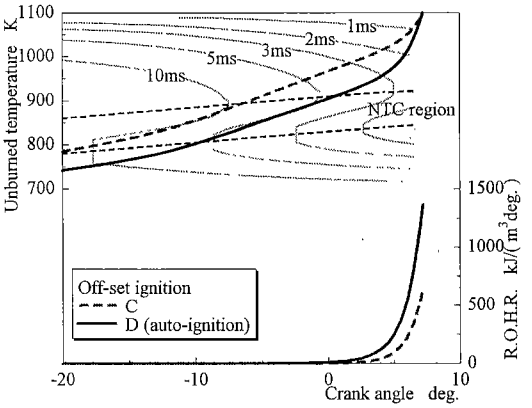

Figure 14 Time histories of temperatures and local heat release rate at a core region cell (location C) and the first local auto-ignition cell (location D); Off-set ignition

The two above-described appearances of the auto-ignition sites are similar to experimentally determined results[(1) ~ (5)] in which the first local auto-ignition is observed in the near-wall regions in some cases and distant from the wall in other cases.

5. Conclusions

The locations of auto-ignition initiation were analyzed by solving the transport equations coupled with a reduced kinetic model for the low-temperature oxidation reaction.

In the first analysis, a compression ignition in a rapid compression machine was solved for a laminar state. The results shows that the vortex induced in a piston-liner corner separates the volume into lower- and higher-temperature regions in a central core and in an outer region from the cylinder axis, respectively. In this condition, the auto-ignition initiates in the outer region when the temperature field is outside the NTC region, and the auto-ignition first appears at the border between the lower- and higher-temperature regions when the temperatures are inside the NTC region.

In the second analysis, the auto-ignition in an S. I. engine was analyzed in a three-dimensional turbulent field by solving the spatially-filtered transport equations to model a randomly fluctuating temperature field. The time of the auto-ignition in the end gas is shown to be in good agreement with the experimentally obtained value. In the central spark case, auto-ignition initiates at several locations distant from the walls, whereas in the offset spark case, the first local auto-ignition appears near the walls; or the lower-temperature location comes earlier to the auto-ignition. It is suggested that the first auto-ignition does not always occur in higher-temperature regions and that the difference in the locations of the first auto-ignition depends on the time period during which the local end gas temperature passes through the region of shorter ignition delay, including the NTC region.

Acknowledgements

This work was supported by Daimler-Chrysler AG, Research and Technology, FT1/T. The authors wish to thank Prof. Dr. R. Maly of Daimler-Chrysler AG for his support and advice.

References

(1) Nakagawa, Y., Takagi, Y, Itoh, T. and Iijima, T., SAE Paper No. 845001.

(2) Hayashi, T, Taki, M., Kojima, S. and Kondo, T., SAE Paper No. 841336.

(3) Konig, G. and Sheppard, C. G. W., SAE Paper No. 902135.

(4) Konig, G., Maly, R. R., Bradly, D., Lau, A. K. C. and Sheppard, C. G. W., SAE Paper No. 902136.

(5) Spicher, U, Schmits, G and Kollmeier, H. P, SAE Paper No. 881637.

(6) Gosman, A. D., Marooney, C. J. and Weller, H. G., Proc. COMODIA 90, pp. 59-64, 1990.

(7) Schapertons, H, Lee, W., SAE Paper No. 850502.

(8) Lee, Y., Pae, S. and Min, K., Proc. Proc. 15th I.C.Engines Symp. (Int.), pp.389-394, 1999.

(9) Cowart, J. S., Keck, J. C., Heywood, J. B., Westbrook, C. K. and Pitz, W. J., 23rd Symp. (Int.) on Combustion/The Combustion Institute, pp.1055-1062,1990.

(10) Nishiwaki, K., Yoshihara, Y. and Saijyo, K., SAE Paper No.2000011897.

(11) Ishikawa, R., Yoshihara, Y., Nishiwaki, K. and Inoue,J., (in Japanese) Proc.13th I.C.Engines Symp., Tokyo, pp.559-564, 1996.

(12) Foin, C., Nishiwaki, K. and Yoshihara, Y., JSAE Review, 20, pp.401-406, 1999.

(13) Halstead, M. P., Kirsch, L. J. and Quinn, C. P., Combustion and Flame, Vol.30, pp.45-60,1977.

(14) Tabaczynski, R. J., Hoult, D. P. and Keck, J. C., J. Fluid Mech., Vol. 42, pp. 249-255, 1970.

(15) Furutani, M. Ohta Y. and Komatsu, K., JSAE Review, Vol. 14,No.2, pp.12-18, 1993.

(16) Weller, H. G., Uslu, S., Gosman, A. D., Maly, R. R., Herweg, R. and Heel, B., Proc.COMODIA94, pp. 719-729.1994

(17) Gulder, O. L., Smallwood, G. J., Wong, R., Snelling, D. R., Smith, R., Deschamps, B. M. and Sautet, J. C., Combustion and Flame, Vol.120, pp.407-416, 2000.

(18) Nishiwaki, K., Proc. COMODIA98, pp.35-43,1998

(19) Ikegami, M., Shioji, M. and Nishimoto K., SAE Paper No. 870372.